Journal of Fluids and Structures (2001) **15,** 399–413
doi:10.1006/jfls.2000.0353, available online at http://www.idealibrary.com on IDEAL®

INTERACTION BETWEEN VORTEX RINGS AND A SEPARATED SHEAR LAYER: TOWARDS ACTIVE CONTROL OF SEPARATION ZONES

M. KIYA, O. MOCHIZUKI AND H. ISHIKAWA

Graduate School of Engineering, Hokkaido University
Sapporo, 060-8628, Japan

(Received 29 August 2000, and in final form 14 November 2000)

The separation zone of an inclined flat plate was reduced by bombarding rolling-up vortices in the separated shear layer with a chain of vortex rings introduced from the side of the main flow. The reduction was realized because a compact and strong vortex is successively formed near the leading edge, transporting high-momentum fluid of the main flow towards the surface. Momentum defect in the near wake, which serves as a measure of effectiveness of reduction in the separation zone and can be approximately interpreted as the drag of the plate, generally decreases with increasing frequency of introduction of the rings F and their circulation Γ, saturating at sufficiently large values of F and Γ. The momentum defect appears to attain a minimum at a particular frequency $Fc/U_\infty \approx 4$, where c is the length of the plate and U_∞ is the main-flow velocity. This frequency can be interpreted as the fundamental frequency of the shedding-type instability of the separated flow. Efficiency, which is defined as decrease in loss of power in the wake divided by the power required to generate the vortex rings, attains a maximum approximately at the same frequency $Fc/U_\infty \approx 4$, and at a particular value of the circulation $\Gamma/U_\infty c \approx 0{\cdot}32$, which is approximately 1·6 times the circulation of the shear-layer vortices in the region of interaction. Thus, the steady jet which corresponds to $F = \infty$ is not the best choice in terms of the efficiency. © 2001 Academic Press

1. INTRODUCTION

ACTIVE CONTROL OF SEPARATED FLOWS around bluff bodies has been made by acoustic wave, suction or blowing, oscillating flaps, moving surfaces, etc. These methods, except the control by acoustic wave, employ actuators installed inside or on the surface of the body. This is not always possible in engineering applications. For example, blades of axial-flow compressors or blowers are not usually thick enough to install such actuators. Active control of separated flow around the blades is of vital importance to improve off-design performance of turbomachinery.

This paper presents a novel method to solve the above problem. In this method self-travelling vortices such as vortex rings or vortex pairs are introduced into separated shear layers from outside to reduce the separation zone. Figures 1 and 2 are flow visualizations which demonstrate the interaction between the external vortices and rolling-up vortices in a separated shear layer (Kiya *et al.*, 1986). Note that the vortex ring and the vortex pair in these figures are introduced from the low-velocity side of the shear layer. The interaction appears to generate rolling-up vortices which are larger than those in the undisturbed shear layer.

The interaction between rolling-up vortices in a plane mixing layer and a vortex pair was studied by numerical simulations to understand essential aspects of the vortex interaction

0889–9746/01/040399 + 15 $35.00/0 © 2001 Academic Press

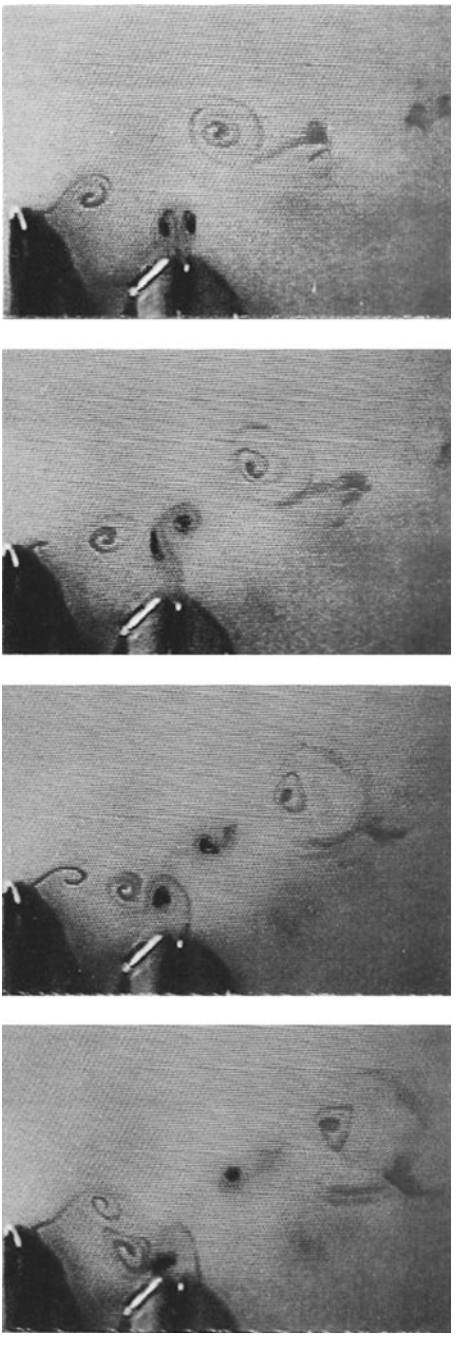

Figure 1. Interaction between a vortex pair and shear-layer vortices (Kiya *et al*., 1986). Flow is from left to right. Main-flow velocity $U_\infty = 2{\cdot}8$ cm/s, height of normal plate $h = 4{\cdot}3$ cm, circulation of the vortex pair $\Gamma_{vp}/(U_\infty h) \approx 0{\cdot}78$, circulation of the shear-layer vortices $\Gamma_{sh}/(U_\infty h) \approx 0{\cdot}50$ and Reynolds number $U_\infty h/\nu = 1{\cdot}2 \times 10^5$. The time interval between two consecutive photographs is 0·5 s.

(Kiya *et al*. 1999). This two-dimensional interaction induces larger vortices than those in the undisturbed mixing layer, yielding a significant increase of momentum thickness and entrainment rate. Moreover, vortex pairs whose circulation is larger than approximately 2·5

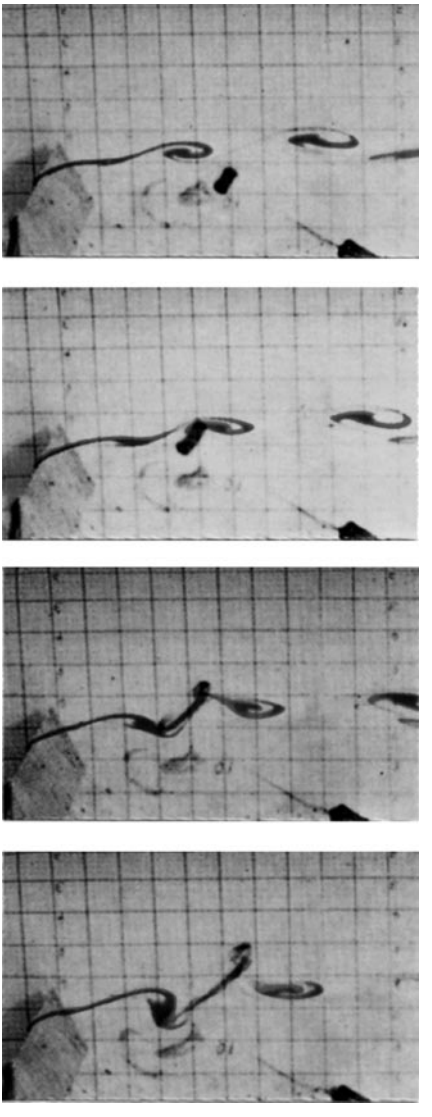

Figure 2. Interaction between a vortex ring and shear-layer vortices (Kiya *et al*., 1986). Flow is from left to right. $U_\infty = 3{\cdot}0$ cm/s, $h = 4{\cdot}3$ cm, circulation of the vortex ring $\Gamma_{vr}/(U_\infty h) \approx 0{\cdot}58$, $\Gamma_{sh}/(U_\infty h) \approx 0{\cdot}85$ The time interval between two consecutive photographs is 0·25 s.

times the circulation of the mixing-layer vortex pass through the mixing layer, leaving more or less the same effect on the mixing-layer vortices.

A problem of using a vortex pair for the control is that it has a mode of instability (Leweke *et al*. 1996), which degenerates the vortex pair to a series of vortex rings. Thus, in engineering applications, the external vortices should be vortex rings. Interaction between vortex rings and shear-layer vortices was studied experimentally by Kiya *et al*. (1986) and Maekawa & Nishioka (1992) and numerically by Kiya & Ishii (1988) and Ishikawa *et al*. (2000). In the Ishikawa *et al*. (2000) simulations, a vortex ring of radius R and core radius of $0{\cdot}155R$ interacts with a rectilinear vortex tube of the same core radius; the Reynolds number based on the diameter $2R$ and the initial convection velocity of the vortex ring is 300. The

simulations revealed that the vortex ring passes through the vortex tube if the circulation of the vortex ring is approximately 1·5 times the circulation of the vortex filament.

In this paper, vortex rings were introduced into the separated shear layer of an inclined flat plate to reduce the height of the separation zone. A reduction in the height is expected to be accompanied by lower drag and higher lift, and lower level of fluctuating components of these forces. Trajectories of vortex rings ejected into the main flow are shown to have a similarity for different parameters associated with generation of the vortex rings (Suzuki *et al.* 1999), and this similarity was used to introduce the vortex rings into the separated shear layer near the leading edge. Circulation of the vortex rings Γ and frequency of its introduction (shooting frequency) F were changed to obtain conditions of the greatest reduction in the separation zone. Momentum defect in the near wake of the plate is employed as a measure of effectiveness of the control. Moreover, the mechanism of the reduction is discussed in terms of phase-averaged flow visualizations and phase-averaged velocity distributions.

2. EXPERIMENTAL APPARATUS AND METHOD

Experiments were performed in a low-speed, open-return wind tunnel with a 40·0 cm high, 20·0 cm wide and 90·0 cm long working section. The flow was introduced into the working section through a bell entrance of 1 : 12·6 contraction. The time-mean velocity in the tunnel was uniform within $\pm 2\%$ in the cross section where the leading edge of a model plate is to be located except the boundary layers on the tunnel walls. The free-stream turbulence intensity was 0·7%.

Vortex rings were produced through a circular orifice of diameter $d = 5{\cdot}0$ mm, which were bored through the top wall of the tunnel in the mid-span plane. This orifice was connected to a woofer through a chamber. In the second part of the experiments, which will be described in Section 3.3, two orifices of the same dimensions were added $6{\cdot}0\,d$ apart, on both sides of the above-mentioned orifice; all the five orifices were arranged along a line normal to the main-flow direction, being connected to the woofer through the same chamber. Thus, five vortex rings of the same circulation and dimensions were generated simultaneously.

The woofer was driven by square-wave input from a power unit. The square wave had a period of $2t_b$; in the first half of the period the woofer was in the phase of ejection flow through the orifice, while in the second half the woofer was in the suction phase.

Circulation of the vortex ring generated during one period was obtained in the following way. The cylindrical coordinate (ξ, σ, φ), whose origin is at the centre of the orifice, is defined such that ξ is the longitudinal distance, σ is the radial distance, and φ is the azimuthal angle about the axis $\sigma = 0$. Assuming that the flow in the plane of the orifice is axisymmetric, circulation shed per unit time from the edge of the orifice is given by

$$\frac{\mathrm{d}\Gamma}{\mathrm{d}t} = \int_{d/2-\delta}^{d/2} \omega_\varphi u_\xi \,\mathrm{d}\sigma, \tag{1}$$

where δ is the thickness of the shear layer, $\omega_\varphi = \partial u_\sigma/\partial\xi - \partial u_\xi/\partial\sigma$ is the azimuthal component of vorticity, and u_ξ and u_σ are the velocity components in the ξ and σ directions. The first term in ω_φ is much smaller than the second term, so that we obtain $\omega_\varphi u_\xi = -u_\xi(\partial u_\xi/\partial\sigma)$. Thus, noting that the flow in the suction phase had no contribution to circulation, the circulation of the vortex ring generated during one period of motion of the woofer can be evaluated from

$$\Gamma = \frac{1}{2}\int_0^{t_b} [V_j(t)]^2 \,\mathrm{d}t, \tag{2}$$

where $V_j(t)$ is the longitudinal velocity component at the edge of the shear layer in the plane of the orifice.

An inclined flat plate of length $c = 100$ mm was made from an acrylic resin plate of 2·0 mm in thickness, having the semicircular leading and trailing edges. This form of the leading edge was employed to reduce the receptivity of the acoustic wave generated by the motion of the woofer. It is possible that the receptivity might influence the rolling up of the

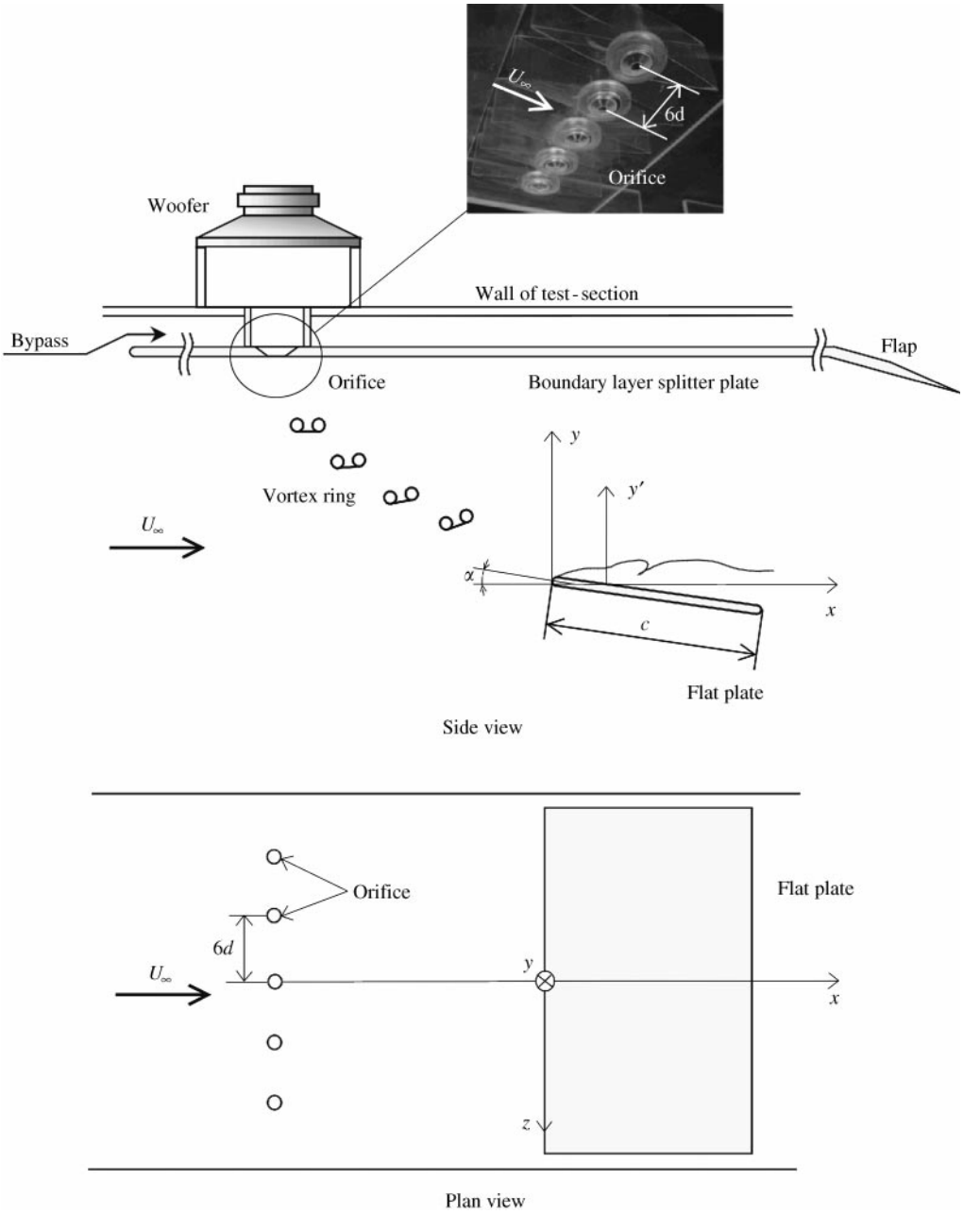

Figure 3. Flow configuration and definition of coordinate system for active control of separation zone of an inclined flat plate by impinging vortex rings.

separated shear layer, making it difficult to differentiate its effects on the separation zone from those of the vortex rings. The plate was fixed at an attack angle $\alpha = 10^\circ$, at which the flow separated from the leading edge to reattach to the surface near the trailing edge.

Figure 3 illustrates the flow configuration, and definition of the (x, y, z) coordinate system and symbols. The x-axis is in the direction of main flow of velocity U_∞, y is vertically upward, and z is in the spanwise direction, the origin being at the leading edge. The distance from the suction surface along the y-axis is denoted by y'. The instantaneous velocity components in the xy-plane and in the x-direction are denoted by q and u, respectively. The leading edge of the plate was located $15{\cdot}0d$ below and $25{\cdot}0d$ downstream of the centre of the orifice from which the vortex rings were generated.

The velocities were measured by a constant-temperature hot-wire anemometer and a Laser-Doppler velocimeter (LDV). A single hot-wire probe of 5 μm diameter and working length of 1 mm, which was parallel to the z-axis, was used, so that this probe measured the velocity component in the (x, y) plane q, whose time-mean value and r.m.s. fluctuations are denoted by $\bar{q}$ and q', respectively. The LDV measured the longitudinal component u, whose time-mean value is denoted by $\bar{u}$.

The vortex rings and their interaction with the separated shear layer were visualized by a smoke-wire technique. Smoke wires were tungsten wires of $0{\cdot}1$ mm diameter with kinks at intervals of $2d$. Flow-visualization photographs were taken in synchronization with fixed phases of generation of the vortex rings.

Reynolds number Re ($= U_\infty c/\nu$, ν being the kinematic viscosity) was 8300. The main-flow velocity was $1{\cdot}25$ m/s. The frequency of introduction of the vortex rings to the separated shear layer F was varied in the range of $Fc/U_\infty = 0$–12, while circulation of the vortex rings was in the range of $\Gamma/(U_\infty c) = 0{\cdot}20$–$0{\cdot}66$. Circulation of shear-layer vortices with which the vortex rings interacted, Γ_{sh}, was $\Gamma_{sh}/(U_\infty c) = 0{\cdot}21$, as described in Section 3.1.

3. RESULTS AND DISCUSSION

3.1. Undisturbed Flow

Figure 4 shows the flow pattern visualized by smoke particles, the distributions of the time-mean velocities $\bar{q}$ and $\bar{u}$ and the r.m.s. velocity fluctuation q' on the suction side of the plate. The flow separates from the leading edge to form a separation zone. The distributions of $\bar{u}$ measured by the LDV indicate the reverse flow near the surface. In the reverse-flow region, the distributions of $\bar{q}$ measured by the hot-wire probe has a definite plateau. The plateau is generated by the rectification of the velocity signal u in the reverse-flow region. Near a position of $u = 0$, the hot-wire signal is expected to attain a broad minimum because the rectification yields a higher signal between this position and the surface. The broad minimum looks like a plateau. It may be noted that the hot-wire signal is not zero at the position of $u = 0$ due to effects of natural convection and the turbulent velocity component along the probe. Thus, in this paper the plateau is interpreted as an indication of reverse flow. On the basis of this interpretation, the separated shear layer appears to reattach on the surface near the trailing edge. This is partially supported by the fact that the distribution of $\bar{u}$ in the near wake at $x/c = 1{\cdot}14$ indicates no reverse-flow region.

Circulation of rolling-up vortices in the undisturbed shear layer Γ_{sh} can be estimated on the basis of the velocity at the edge of the shear layer $U_s (= 1{\cdot}27U_\infty$ at $U_\infty = 1{\cdot}25$ m/s) and the fundamental frequency of Kelvin–Helmholtz instability $f_{KH} = 50$ Hz, which was measured at $x/c = 0{\cdot}4$. As seen in Figure 4, the rolling-up vortex in the shear layer first appears between $x/c = 0{\cdot}3$ and $0{\cdot}4$. The longitudinal distance between rolling-up vortices near the

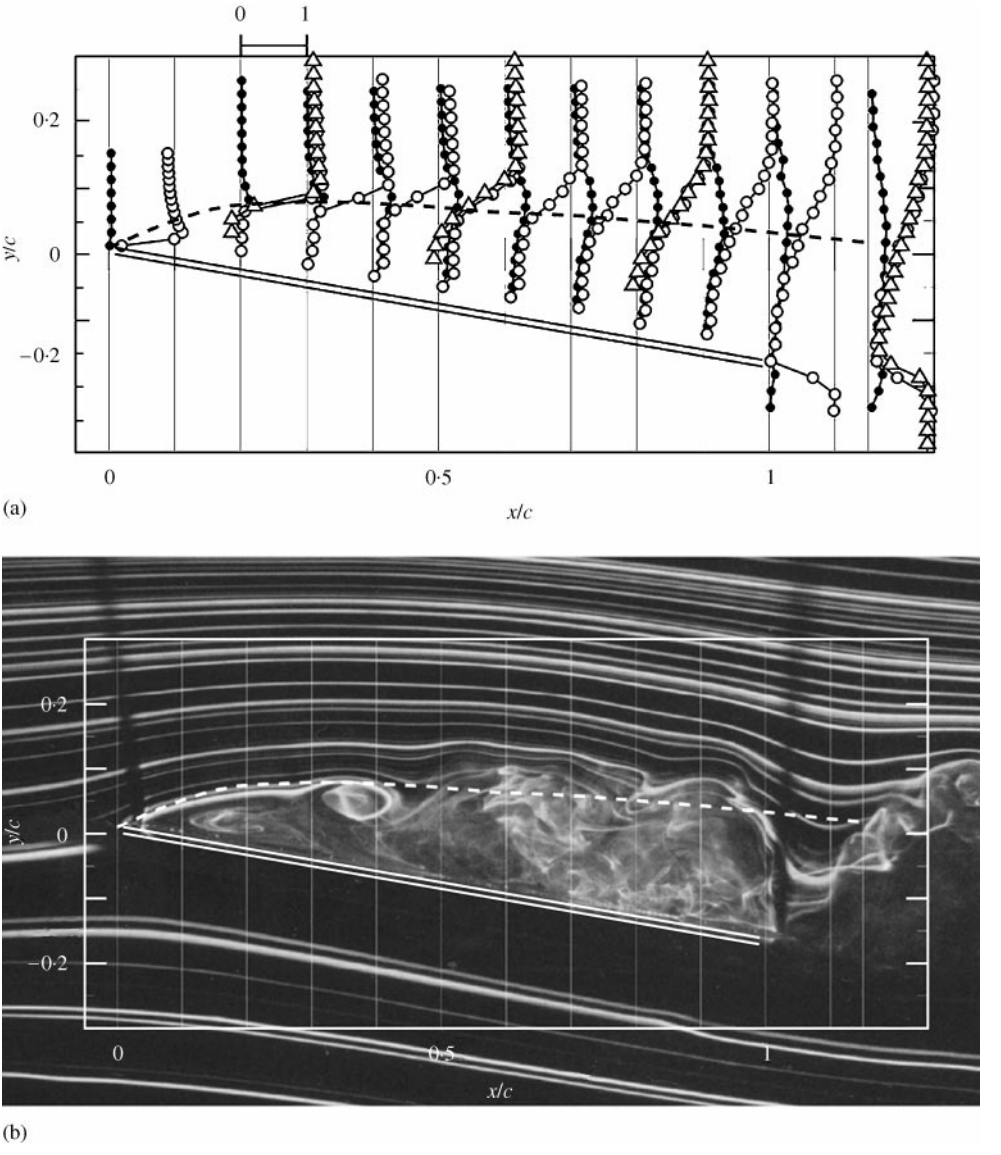

Figure 4. (a) Distributions of time-mean velocities $\bar{q}$ and $\bar{u}$, and r.m.s. velocity fluctuation q', and (b) smoke-wire flow visualization for undisturbed separation zone. $\alpha = 10^\circ$ and Re = 8300. ○, $\bar{q}/U_\infty$; △, $\bar{u}/U_\infty$; ●, q'/U_∞. The broken line shows the centre of the shear layer. The scale of the velocities is shown on top of (a).

leading edge (which will be referred to as KH vortices) is estimated as $\lambda_{KH} = (U_s/2)/f_{KH}(= 0{\cdot}16c)$, with the reasonable assumption that the rolling-up vortices are convected by the velocity $U_s/2$. Circulation of the shear layer vortices can be estimated as U_s times this wavelength, that is, $\Gamma_{sh}/(U_\infty c) = 0{\cdot}21$.

3.2. Effects of Vortex Rings on Separated Flow

In order to demonstrate the effects of vortex rings on the shear layer, phase-averaged flow visualizations and distributions of phase-averaged velocity $\tilde{q}$ are presented in Figures 5 and 6

for the shooting frequency of $Fc/U_\infty = 0{\cdot}80$. The vortex rings were generated only from the central orifice; the flow visualizations and the velocity measurements were made in the mid-span plane. The phase averaging was made on the basis of waveform of input to the woofer. For convenience the phase $\phi = 0$ is defined as the instant at which the centre of a vortex ring arrives at the leading edge of the airfoil, while the phase $\phi = 2\pi$ is the instant at which the next vortex ring arrives at the same position. The velocity distributions and the flow visualizations are shown with the interval of $\Delta\phi = \pi/3$. It may be noted that each photograph of Figure 5 is the superposition of 20 realizations; the centre of the vortex ring is indicated by solid triangles on the longitudinal and horizontal scales. The phase-averaged velocity distributions are also the superposition of 20 realizations. It is also worth noting that position of the vortex rings was much clearer in each flow realization than that in the phase-averaged visualization.

The flow patterns in Figure 5 demonstrate the process of interaction between the shear layer and the vortex ring. The vortex ring impinges on the shear layer near the leading edge at $\phi = \pi/3$, generating a compact rolling-up vortex whose centre is at $x/c \approx 2{\cdot}5$ for $\phi = 2\pi/3$ [Figure 5(c)]. This compact vortex eliminates the reverse flow on its downstream side to reduce the instantaneous length of the separation zone, as seen from the velocity profile at $x/c = 0{\cdot}4$, by transporting high-momentum fluid of the main flow towards the surface. At the same time, the centre of the shear layer y_c, which is the y position of maximum of q', shifts towards the surface, yielding a dip in the plot of y_c against x.

This compact vortex grows in size downstream to make the shear layer reattach at a position $x/c \approx 0{\cdot}5 - 0{\cdot}6$ at $\phi = \pi$ [Figure 5(d)]. The x coordinate of the reattachment position is indicated by the open triangle. As the interaction zone moves downstream, the reattachment position and the dip of y_c also move downstream. At the last phase $\phi = 5\pi/3$ [Figure 5(f)], the reattachment position the dip are located further downstream at $x/c \approx 0{\cdot}7$; the next vortex ring is approaching the leading edge to yield the same pattern as that at $\phi = 0$.

It is worth noting that the motion of the dip is preceded by the motion of the vortex ring (Figure 6). The convection velocity of the dip is estimated to be approximately $0{\cdot}50\,U_s$, while the convection velocity of the vortex ring is estimated to be $0{\cdot}91U_s$. This means that the dip is actually caused by the local enhancement of rolling-up of the shear layer by the interaction with the vortex ring. This also suggests that the longitudinal motion of the vortex rings are affected by its self-induced velocity because the vortex rings travel downstream along the suction surface.

Effects of the shooting frequency F on distributions of the time-mean and r.m.s. velocities are shown in Figure 7 for two shooting frequencies $Fc/U_\infty = 0{\cdot}80$ and $5{\cdot}6$. The ratio of circulation is in the range of $\Gamma/\Gamma_{sh} = 2{\cdot}5$–$3{\cdot}6$, so that, in view of the numerical simulations (Kiya *et al.*, 1999; Ishikawa *et al.*, 2000), the vortex rings are expected to pass through the shear layer. Figure 7 also indicates that the separated shear layer approaches the suction

Figure 5. Flow visualization of the separated flow affected by the impinging vortex rings for $Fc/U_\infty = 0{\cdot}80$ and $\Gamma/(U_\infty c) = 0{\cdot}67$. Flow is from left to right. Phase is $\phi = 0$ in (a) and $\phi = 5\pi/3$ in (f) with the same interval of $\pi/3$ between succesive snapshots. The phase-averaged reattachment position is indicated by the open triangles. Coordinates of position of the vortex rings are denoted by the solid triangles on the x- and y-axes.

Figure 6. Phase-averaged velocity distributions $\tilde{q}$ in the separated flow affected by the impinging vortex rings for $Fc/U_\infty = 0{\cdot}80$ and $\Gamma/(U_\infty c) = 0{\cdot}67$. Flow is from left to right. Phase is $\phi = 0$ in (a) and $\phi = 5\pi/3$ in (f) with the same interval of $\pi/3$ between successive snapshots. The phase-averaged reattachment position is indicated by the open triangles. Coordinates of the position of the vortex rings are denoted by the solid triangles on the x- and y-axes. Thin solid lines indicate the distributions of the time-averaged velocity $\bar{q}$ in the undisturbed shear layer, while the thick solid lines show the centre of the shear layer affected by the vortex rings.

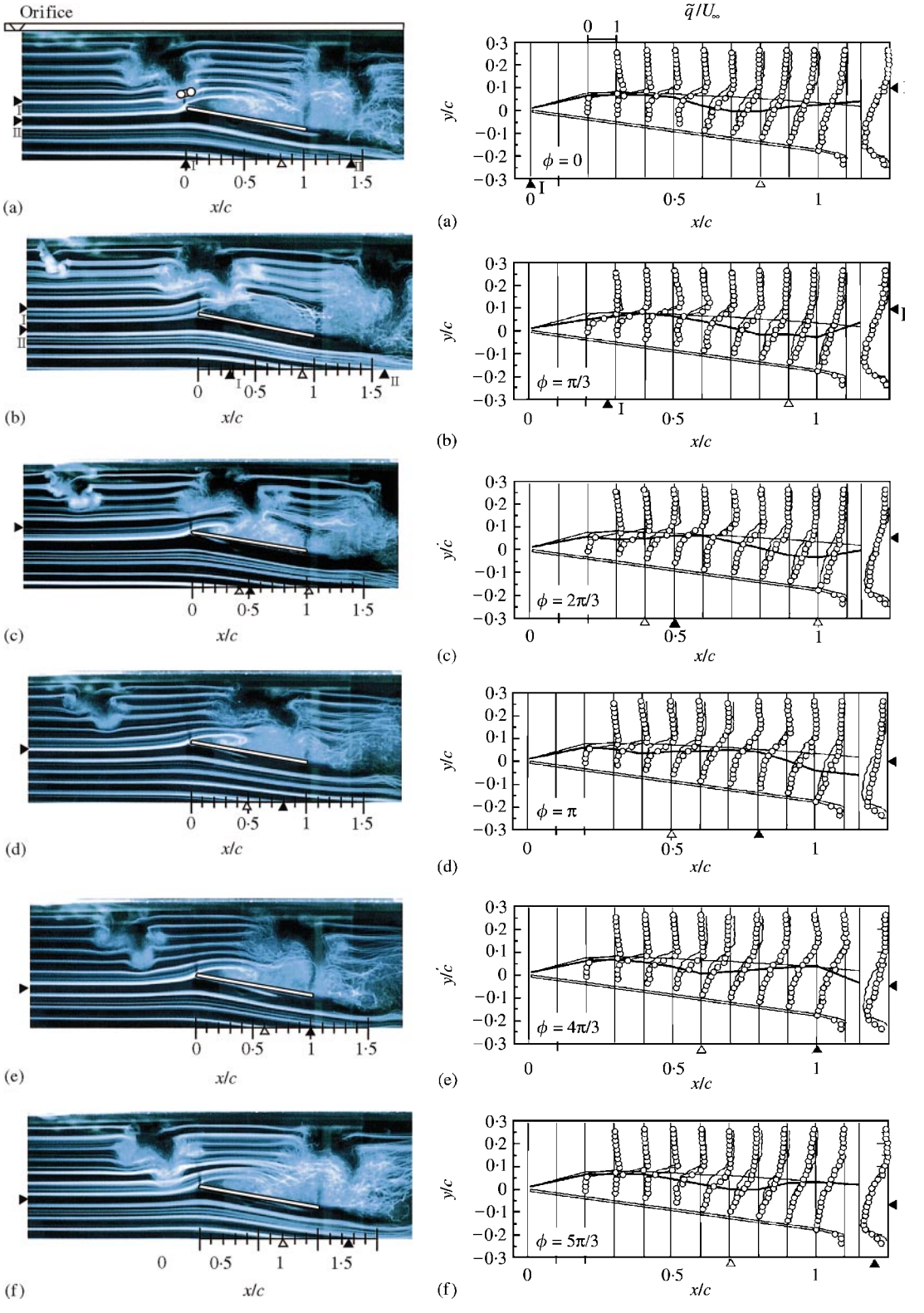
Orifice
$\tilde{q}/U_\infty$
(a)
(b)
(c)
(d)
(e)
(f)
x/c
y/c
$\phi = 0$
$\phi = \pi/3$
$\phi = 2\pi/3$
$\phi = \pi$
$\phi = 4\pi/3$
$\phi = 5\pi/3$

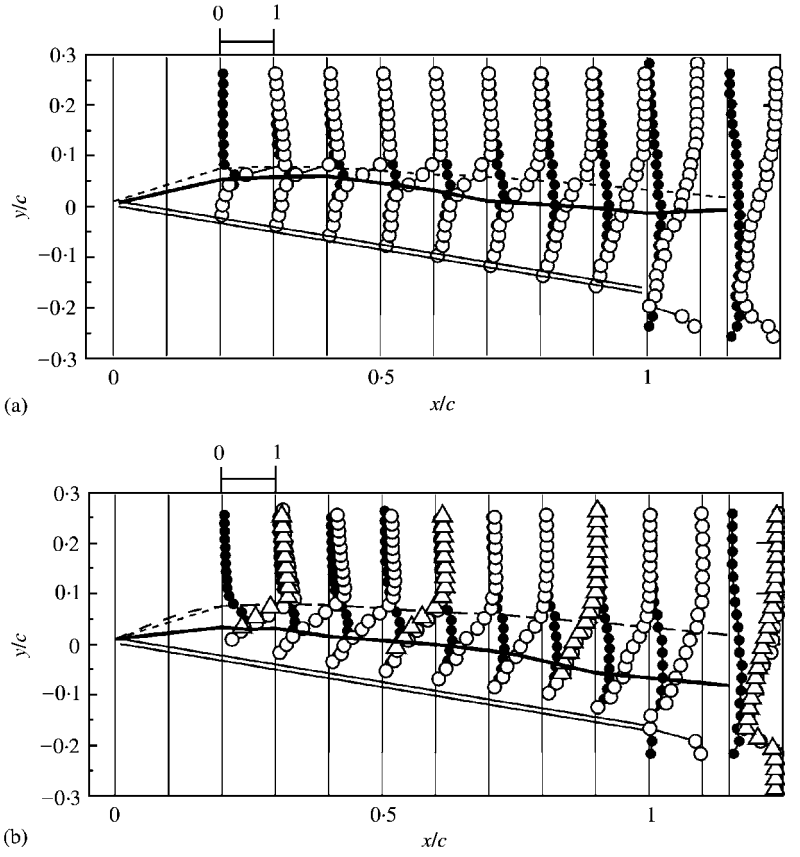

Figure 7. Effects of the impinging vortex rings on the separated flow around the inclined flat plate for (a) $Fc/U_\infty = 0{\cdot}80$, $\Gamma/(U_\infty c) = 0{\cdot}73$ and (b) $Fc/U_\infty = 5{\cdot}6$, $\Gamma/(U_\infty c) = 0{\cdot}50$: △, $\bar{u}/U_\infty$; ○, $\bar{q}/U_\infty$; ●, q'/U_∞. The scale of the velocities is shown on top of (a) and (b).

surface as the frequency F increases. Especially, at the frequency $Fc/U_\infty = 5{\cdot}6$, the separation zone is likely to be suppressed.

Effects of the frequency F on time histories of the instantaneous velocity q in the shear layer are shown in Figure 8. The time histories are measured at a fixed position $(x/c, y'/c) = (0{\cdot}5, 0{\cdot}13)$, which is approximately the centre of the undisturbed shear layer. For example, the time history for $Fc/U_\infty = 0{\cdot}80$ is periodic; its time-mean value is approximately 68% greater than that for the undisturbed shear layer. This increase is due to the above-mentioned shift of the shear layer towards the suction surface. The time at which a peak of q appears corresponds to the phase ϕ at which the dip of the centre of the shear layer y_c locates right at the longitudinal position of $x/c = 0{\cdot}5$ (Figure 6).

As the frequency F increases further up to $Fc/U_\infty = 5{\cdot}2$, the time-mean value of q increases to attain a value almost equal to U_∞ (Figure 8). At the same time, the time history of q for this frequency is random, containing no periodic component corresponding to the frequency F. Thus, at sufficiently high shooting frequencies F, the effects of the vortex rings are expected to be the same as those of the steady round jet of the same momentum. On the other hand, at a low frequency $Fc/U_\infty = 0{\cdot}08$, the time-mean value of q is the same as that

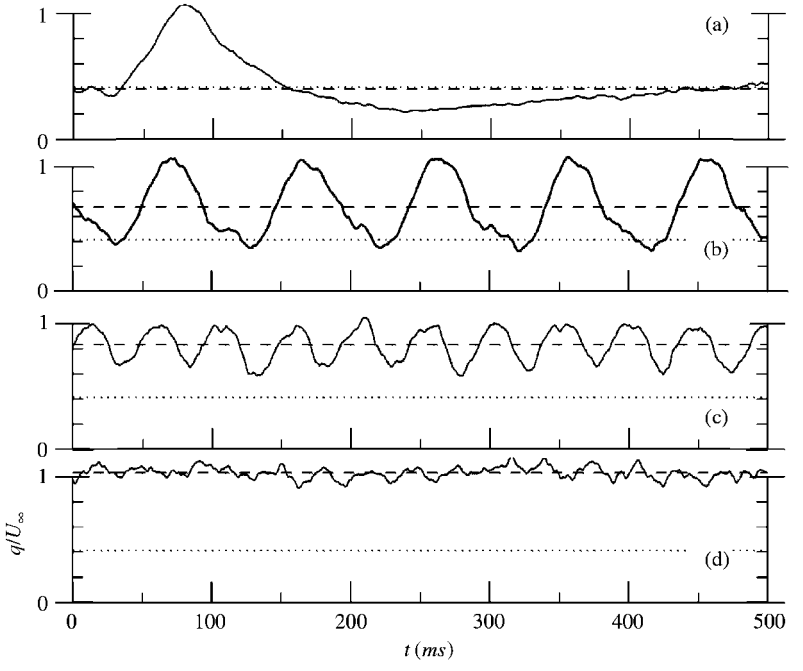

Figure 8. Time histories of velocity q in the shear layer at ($x/c = 0{\cdot}5$, $y'/c = 0{\cdot}13$) for different shooting frequencies F: (a) $Fc/U_\infty = 0{\cdot}08$; (*b*) $Fc/U_\infty = 0{\cdot}80$; (*c*) $Fc/U_\infty = 1{\cdot}60$; (*d*) $Fc/U_\infty = 5{\cdot}20$. $\Gamma/(U_\infty c) = 0{\cdot}67$. The broken lines are the time-mean velocity $\bar{q}$, while the dotted lines is the time-mean velocity $\bar{q}$ at the same position in the undisturbed shear layer.

for the undisturbed flow, so that the vortex rings introduced at this frequency have an insignificant effect on the separated shear layer.

3.3. Momentum Defect in The Near Wake

The previous results are for the vortex rings generated from a single orifice whose centre is at mid-span, the measurements having been made in the mid-span plane. In the following, results will be presented for the vortex rings simultaneously generated from the five orifices arranged in the spanwise direction with the distance 6*d*, as described in Section 2, in order to have fairly two-dimensional interaction between the vortex rings and the shear layer. The distance of 6*d* was employed because the time-mean velocity contours in the *yz*-plane, for the single orifice, were two-dimensional in the near wake within the spanwise distance of $\pm 3d$. The velocity contours in the *yz*-plane for the simultaneously generated five vortex rings were found to be fairly two-dimensional at $x/c = 1{\cdot}15$ (Suzuki *et al.*, 1999).

A measure of effects of the vortex rings impinging on the separated flow is the drag acting on the inclined plate. In the present study the drag was evaluated in terms of the momentum defect in the near wake of the plate, neglecting the contribution of pressure. High momentum defect in the near wake is associated with low pressure there, so that high momentum defect implies high drag. The momentum defect M is defined by

$$M = \int \rho \bar{u}(U_\infty - \bar{u})\,\mathrm{d}y, \tag{3}$$

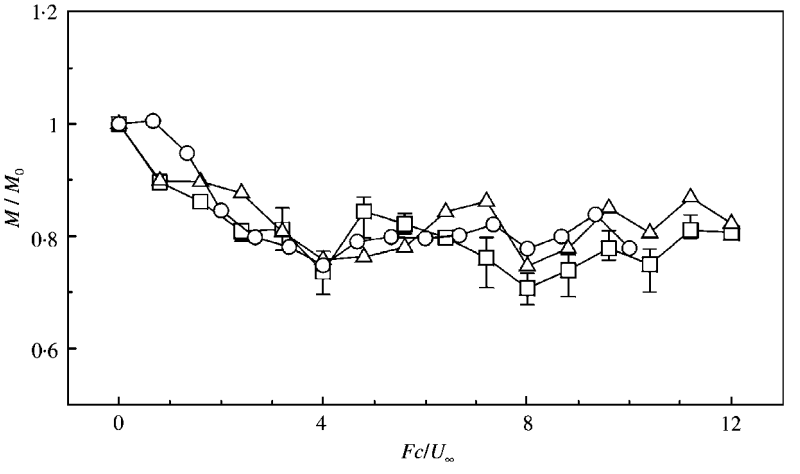

Figure 9. Momentum defect M versus the shooting frequency F for vortex rings issuing from five orifices arranged in the spanwise direction with a distance of $6{\cdot}0d$: ○, $\Gamma/(U_\infty c) = 0{\cdot}23$; △, $\Gamma/(U_\infty c) = 0{\cdot}29$; □, $\Gamma/(U_\infty c) = 0{\cdot}36$.

where ρ is the density of fluid. Figure 9 shows the momentum defect M in the mid-span plane at at $x/c = 1{\cdot}15$, divided by its value of the undisturbed flow M_0, as a function of the shooting frequency F. The momentum defect initially decreases with increasing F to attain a fairly constant value of $M/M_0 = 0{\cdot}8$ for $Fc/U_\infty > 4{\cdot}0$. However, a perusal of Figure 9 reveals that the momentum defect attains a definite minimum at $Fc/U_\infty \approx 4{\cdot}0$. This is the same even when the main-flow velocity has been changed by the factor of 2, as shown in Figure 10.

The particular frequency $Fc/U_\infty = 4{\cdot}0$ can be explained as follows. Periodic forcing of stalled flow around two-dimensional airfoils yields a particular forcing frequency, F_p, at which the lift attains a maximum (Hsiao *et al*., 1989; Bar-Sever 1989; Zaman & McKinzie 1991; Zaman 1992). The drag is also expected to attain a minimum value at the same frequency because the height of the separated zone becomes minimum. This frequency when normalized in the form $F_p c/U_\infty$ is in a range of 3–4 (Zaman & McKinzie 1991; Zaman 1992), 1–3 (Hsiao *et al*., 1989) and 2 (Bar-Sever 1989), being of the same order as the above-mentioned frequency $Fc/U_\infty = 4$. At high Reynolds numbers the frequency F_p is much lower than the fundamental frequency of Kelvin–Helmholtz (K–H) instability in the separated shear layer F_{KH} (Zaman 1992). Nishioka *et al*. (1990) found that the forcing by acoustic waves of low amplitude amplifies the fundamental mode of the linear instability, whereas high amplitude forcing amplifies the mode of much lower frequency. The primary mechanism is likely to be the shedding-type instability (Nishioka *et al*., 1990; Sigurdson 1995) whose frequency scales with the height of the separation zone and the velocity at the separation edge U_s. The mechanism is also interpreted as the impinging-type instability (Nakamura & Nakashima 1986; Kiya *et al*., 1997).

At sufficiently low Reynolds numbers the frequency of the shedding-type instability is perhaps of the same order as that of the K–H instability because vortices rolled-up by the K–H instability can be shed downstream without further merging. This is probably the case in the present experiment at $\mathrm{Re} = 8300$ because the frequency $Fc/U_\infty = 4$ happens to be that of the K–H frequency at $x/c = 0{\cdot}4$. A similar relation is observed between the frequency of the shear layer instability and that of the column-type instability of a round jet (Ho & Huerre 1984).

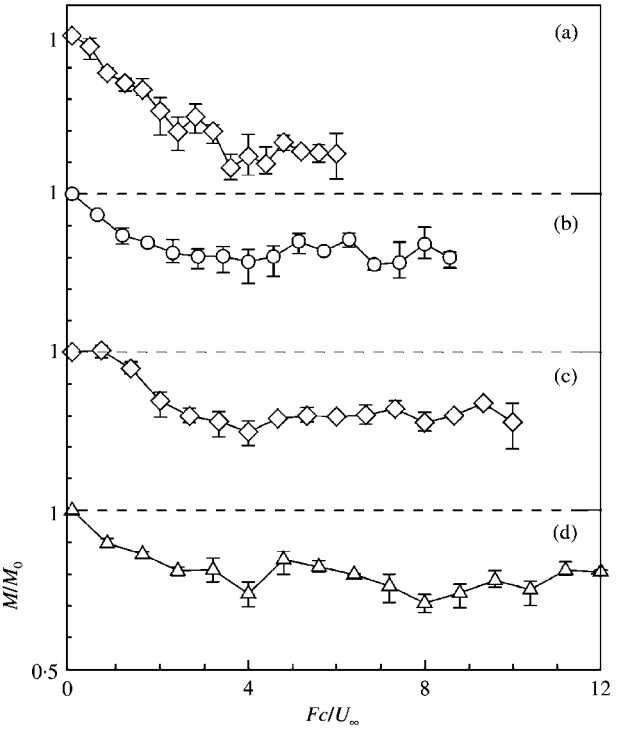

Figure 10. Momentum defect M versus the shooting frequency F at (a) Re = 16600, $\Gamma/(U_\infty c) = 0{\cdot}34$; (b) Re = 11600, $\Gamma/(U_\infty c) = 0{\cdot}48$; (c) Re = 100000, $\Gamma/(U_\infty c) = 0{\cdot}56$; (d) Re = 8300, $\Gamma/(U_\infty c) = 0{\cdot}67$ for the vortex rings issuing from five orifices.

At the optimum frequency $Fc/U_\infty = 4$, the distance between the centre of the consecutive interaction zones is approximately $0{\cdot}16c$ because the convection velocity of the interaction zone is $0{\cdot}51U_s$ ($= 0{\cdot}65U_\infty$). The diameter of the vortex ring is approximately $1{\cdot}5d$ ($= 0{\cdot}075c$), so that the interaction zone is just sufficient to accommodate one vortex ring.

As mentioned before, the momentum defect becomes fairly constant at the shooting frequencies in the range of $Fc/U_\infty > 4{\cdot}0$ (Figure 9). At these frequencies there is no inherent instability in the shear layer to be enhanced by the interaction with the vortex rings. The primary mechanism for the constant value of M should be attributed to an increase in the longitudinal momentum due to the vortex rings. The momentum of the vortex rings is basically in the normal (y) direction but this is converted to the longitudinal momentum by their impingement on the surface.

Effects of circulation of the vortex rings on M are shown in Figure 11. The momentum defect decreases with increasing circulation Γ but is likely to become constant at sufficiently high values of Γ. The latter is probably because such vortex rings pass through the separated shear layer, leaving more or similar effects on the rolling up of the shear layer, as suggested by the numerical simulations (Kiya *et al.*, 1999; Ishikawa *et al.*, 2000).

It may be noted here that, for signal vortex rings, the momentum defect decreased with increasing frequency F (not shown), attaining a fairly constant value of $M/M_0 = 0{\cdot}8$ for $Fc/U_\infty > 6$. This is the same as in the case of arrays of vortex rings. The main difference is that no significant minimum appeared at $Fc/U_\infty \approx 4{\cdot}0$ for the single vortex rings. This is probably because the single vortex rings modified only a limited spanwise region of the

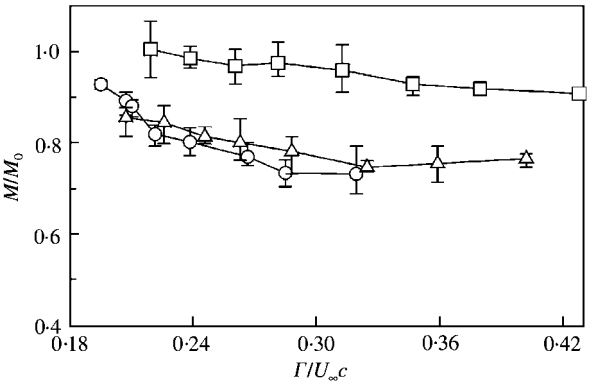

Figure 11. Momentum defect M versus circulation of the vortex rings issuing from five orifices: □, $Fc/U_\infty = 0{\cdot}80$; △, $Fc/U_\infty = 4{\cdot}0$; ○, $Fc/U_\infty = 8{\cdot}0$.

rolling-up vortices in the shear layer, which were otherwise fairly two-dimensional, and thus the two-dimensional shedding-type instability was not enhanced.

3.4. Efficiency of Separation Control by Vortex Rings

Loss of power by the drag acting on the plate is the drag multiplied by the main-flow velocity. The drag of the plate is reduced by the impinging vortex rings; this reduction is accompanied by a reduction in loss of power ΔW. Thus, the efficiency of control can be evaluated by $\eta = \Delta W/W_{vr}$, where W_{vr} is the power of generation of the vortex ring. The kinetic energy of the vortex ring K_{vr} is given by

$$K_{vr} = \frac{1}{2}\rho A_0 \int_0^{t_b} [V(t)]^3 \, \mathrm{d}t, \tag{4}$$

where $A_0 = \pi d^2/4$ is the area of the orifice. The vortex ring is generated with frequency F and the number of the vortex rings per unit length of the span is $1/(6d)$. Thus the power, per unit length, of generation of the vortex rings is $W_{vr} = (F/6d)K_{vr}$. On the other hand, the reduction in loss of power per unit length by the control is given by $\Delta W = U_\infty(M_0 - M)$.

The efficiency η is shown in Figure 12 as a function of the normalized frequency Fc/U_∞ and circulation $\Gamma/(U_\infty c)$. It is noteworthy that a maximum of η appears at a frequency centred around $Fc/U_\infty \approx 4$. Thus the steady round jet, which corresponds to $Fc/U_\infty = \infty$, is not the best choice for the control in terms of the efficiency. Moreover, the efficiency attains a maximum at a particular value of $\Gamma/(U_\infty c) \approx 0{\cdot}32$, which is approximately 1·5 times that of shear layer vortices. It is worth noting that the value of this ratio is equal to the critical value for which a vortex ring passes through a rectilinear vortex tube (Ishikawa *et al.*, 2000).

4. CONCLUSION

In this paper, vortex rings were successively introduced into the separated shear layer of an inclined flat plate to reduce the spatial extent of the separation zone. The circulation and frequency of successive introduction of the vortex rings were changed to examine their effects on the reduction of the separation zone. The main results of this study may be

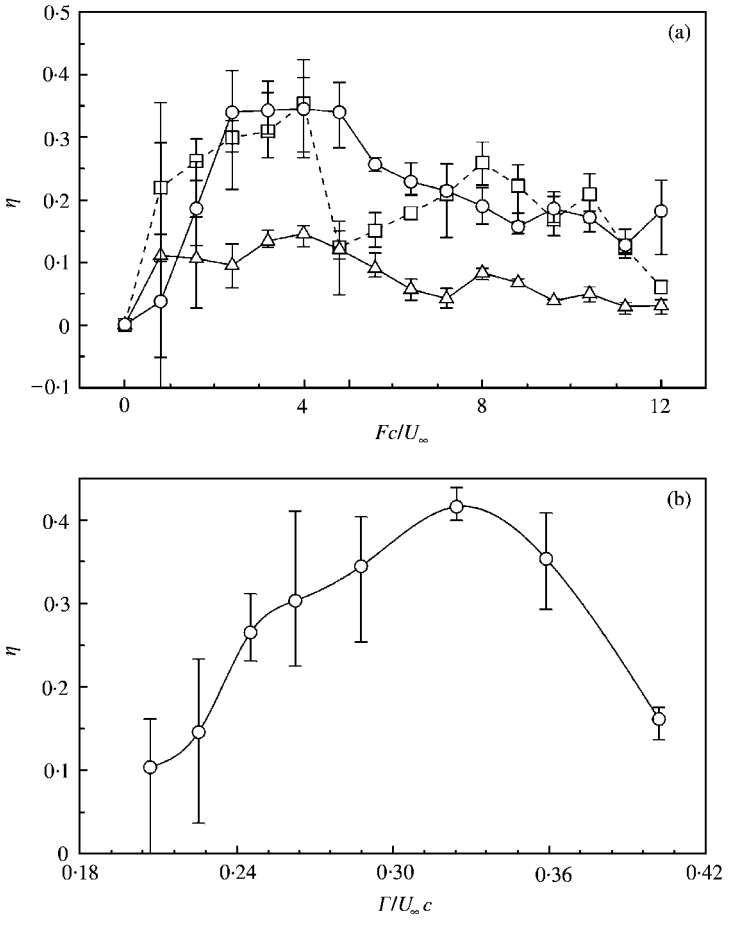

Figure 12. Efficiency of the active control of separation zone η versus (a) the shooting frequency F and (b) the circulation of the vortex rings Γ at $Fc/U_\infty = 4{\cdot}0$: △, $\Gamma/(U_\infty c) = 0{\cdot}22$; ○, $\Gamma/(U_\infty c) = 0{\cdot}27$; □, $\Gamma/(U_\infty c) = 0{\cdot}32$.

summarized as follows.

(i) The separation zone can be reduced by a chain of vortex rings impinging on the shear layer. This is because a compact and strong vortex is successively formed near the leading edge to transport high-momentum fluid of the main flow towards the surface.

(ii) The momentum defect in the near wake of the plate, which is approximately proportional to the drag, is introduced as a measure of effectiveness of active control by the impinging vortex rings. The momentum defect decreases with increasing frequency of introduction of the vortex rings F, saturating at frequencies greater than $Fc/U_\infty \approx 4$. At this particular frequency, the momentum defect appears to attain a minimum value. This optimum frequency is of the order as the frequency at which the lift attains a maximum by periodic forcing of stalled flow around airfoils, suggesting that the impinging vortex rings enhance the shedding-type instability of the separated flow.

(iii) In the present experiment at Reynolds number of 8300, the optimum frequency happens to be approximately equal to the fundamental frequency of Kelvin–Helmholtz instability of the separated shear layer. At higher Reynolds numbers, the optimum frequency $Fc/U_\infty \approx 4$ is expected to be much lower than the Kelvin–Helmholtz frequency.

(iv) There exists a particular value of circulation of the vortex rings beyond which the momentum defect attains a constant value. This is because such vortex rings pass through the separated shear layer, leaving more or less the same effects on the rolling up of the shear layer.

(v) The efficiency of reduction of the separation zone attains a broad maximum approximately at the frequency $Fc/U_\infty = 4$ and at a particular value of circulation of the vortex ring. The former implies that the steady round jet is not the best choice for the control in terms of efficiency.

ACKNOWLEDGEMENTS

The authors express their sincere thanks to Mr Toshiyuki Sampo for his help in the construction of the experimental apparatus. This study was financially supported by the Grant-in-Aid for Scientific Research from the Ministry of Education, Science and Culture, Japan (Category (A)(2), No. 11305016).

REFERENCES

BAR-SEVER, A. 1989 Separation control on an airfoil by periodic forcing. *AIAA Journal* **27,** 820–821.

HSIAO, F., LIU, C., SHYU, J. & WANG, M. 1989 Control of wall-separated flow by internal acoustic excitation. AIAA Paper 89-0974.

HO, C.-M. & HUERRE, P. 1984 Perturbed free shear layers. *Annual Review of Fluid Mechanics* **16,** 365–424.

ISHIKAWA, H., IZAWA, S. & KIYA, M. 2000 Lagrangian LES and vortex dynamics of forced unsteady jets and colliding vortices. In *Advances in Turbulence VIII* (eds C. Topazo *et al.*), pp. 825–828. Barcelona: International Center for Numerical Methods in Engineering.

KIYA, M. & ISHII, H. 1988 Vortex dynamics simulation of interacting vortex rings and filaments. *Fluid Dynamics Research* **3,** 197–202.

KIYA, M., OHYAMA, M. & HUNT, J. C. R. 1986 Vortex pairs and rings interacting with shear-layer vortices. *Journal of Fluid Mechanics* **172,** 1–15.

KIYA, M., SHIMIZU, M. & MOCHIZUKI, O. 1997 Sinusoidal forcing of a turbulent separation bubble. *Journal of Fluid Mechanics* **342,** 119–139.

KIYA, M., TAKEO, H., MOCHIZUKI, O. & KUDO, D. 1999 Simulating vortex pairs interacting with mixing-layer vortices. *Fluid Dynamics Research* **24,** 61–79.

LEWEKE, T., MILLER, G. D. & WILLIAMSON, C. H. K. 1996 Instability in trailing vortices in the temporal development of vortex pairs. In *Advances in Turbulence VI* (eds S. Gavrilakis *et al.*), pp. 361–364. Dordrecht: Kluwer Academic Publishers.

MAEKAWA, H. & NISHIOKA, T. 1992 Control of mixing layer developing structures using a vortex ring. *Transactions of JSME* **58,** 2659–2666 (in Japanese).

NAKAMURA, Y. & NAKASHIMA, M. 1986 Vortex excitation of prisms with elongated rectangular, H and ⊢ cross sections. *Journal of Fluid Mechanics* **163,** 149–169.

NISHIOKA, M., ARAI, M. & YOSHIDA, S. 1990 Control of flow separation by acoustic excitation. *AIAA Journal* **28,** 1905–1915.

SIGURDSON, L. W. 1995 The structure and control of a turbulent reattaching flow. *Journal of Fluid Mechanics* **289,** 139–165.

SUZUKI, N., MOCHIZUKI, O. & KIYA, M. 1999 A pulsating round jet ejected into cross flow. In *Proceedings of International Conference on Fluid Engineering* **I** - *The JSME Centennial Grand Congress*, pp. 129–134. Tokyo: The Japan Society of Mechanical Engineers.

ZAMAN, K. B. M. Q. 1992 Effect of acoustic excitation on stalled flows over an airfoil. *AIAA Journal* **30,** 1492–1499.

ZAMAN, K. B. M. Q. & MCKINZIE, D. J. 1991 Control of laminar separation over airfoils by acoustic excitation. *AIAA Journal* **29,** 1075–1083.